

ARTICLE

DOI: 10.1038/s41467-018-03752-5

OPEN

Rolling up transition metal dichalcogenide nanoscrolls via one drop of ethanol

Xueping Cui^{1,2}, Zhizhi Kong¹, Enlai Gao³, Dazhen Huang^{1,2}, Yang Hao^{1,2}, Hongguang Shen^{1,2}, Chong-an Di¹, Zhiping Xu³, Jian Zheng¹ & Daoben Zhu¹

Two-dimensional transition metal dichalcogenides (TMDs) have attracted lots of interest because of their potential for electronic and optoelectronic applications. Atomically thin TMD flakes were believed capable to scroll into nanoscrolls (NSs) with distinct properties. However, limited by mechanical strength and chemical stability, production of high-quality TMD NSs remains challenging. Here, we scroll chemical vapor deposition-grown monolayer TMD flakes into high-quality NSs *in situ* in 5 s with a nearly 100% yield by only one droplet of ethanol solution. An obvious photoluminescence is demonstrated in NSs and the self-encapsulated structure makes NSs more insensitive to external factors in optical and electrical properties. Furthermore, based on the internal open topology, NSs hybridized with a variety of functional materials have been fabricated, which is expected to confer TMD NSs with additional properties and functions attractive for potential application.

¹ Beijing National Laboratory for Molecular Sciences, Key Laboratory of Organic Solids, Institute of Chemistry, CAS, Beijing 100190, China. ² University of Chinese Academy of Sciences, Beijing 100049, China. ³ Department of Engineering Mechanics and Center for Nano and Micro Mechanics, Applied Mechanics Laboratory, Tsinghua University, Beijing 100084, China. Correspondence and requests for materials should be addressed to J.Z. (email: zhengjian@iccas.ac.cn)

Atomically two-dimensional (2D) transition metal dichalcogenides (TMDs), such as MoS₂, MoSe₂, WS₂, and WSe₂, display numerous exceptional electronic and optical properties arising from quantum confinement^{1,2}. Complementary to gapless graphene, 2D TMDs with intrinsic band gaps are promising interesting field-effect transistor (FET) and optoelectronic devices. Recently, the main focus of attention has been for the production of their intrinsic or heterojunction structures, their properties, and their applications on 2D scale^{3–8}. In addition to changes in 2D size and form, self-assembly of the atomically thin TMD flakes, as an emerging area, is largely unexplored. Assembly processes by folding and scrolling, i.e., rolling up, can transform relatively simple structures into complex topologies, such as nanoscrolls (NSs), with distinct properties as well as the original excellent characteristics. Indeed, theoretical calculations have predicted the unique topology of 2D material-based NSs to yield unusual electronic and optical properties^{9–12}; thus these NSs have promise as building blocks in flexible electronics, microfluidics, energy storage, self-propelled micromachines, and optical resonators^{13–18}. However, experimental realization of such high-quality NSs has only been achieved for graphene^{13–16} and boron nitride¹⁹, which exhibited high strength and chemical inertness. Limitations in mechanical strength and chemical stability present difficulties in producing high-quality TMD-NSs²⁰. Recently, an argon plasma-assisted method has been demonstrated for the fabrication of amorphous MoS₂-NSs, but in this method MoS₂ sheets failed to scroll effectively, only edge region of the sheet curved while the large central area remains plane. Moreover, upon argon plasma etching, a serious damage has been brought to the original sheets, where almost half of sulfur atoms were removed. The obtained NSs exhibited low crystallinity even to be amorphous²¹. A high-quality TMD-NS is highly desirable for both fundamental studies and potential applications; however, its reliable experimental fabrication still remains challenging.

Here, we show a very simple method for fabricating high-quality TMD-NSs, which only requires one droplet of ethanol solution to scroll chemical vapor deposition (CVD)-grown monolayer TMD flakes *in situ* in 5 s with a nearly 100% yield. TMD-NSs are promising optoelectronic materials with potential applications in optoelectronic devices because of the high FET mobility. Owing to self-encapsulated structure, the optical and electrical properties of NSs are more insensitive to external factors, while the electrical performance of 2D materials flakes varies with both the underlying substrate and the environment. In addition, because of the internal open topology, the interlayer

spacing of TMD-NSs can be easily expanded to accommodate a variety of functional materials, including organic small molecules, polymers, nanoparticles, and 2D materials, as well as biological substances. These features are very attractive for applications in solar cells, photodetectors, flexible logic circuits, energy storage, and sensors.

Results

Rolling up CVD-grown TMD monolayer flakes. In a typical experiment, large-area, monolayer TMD flakes were synthesized on a SiO₂/Si substrate by CVD. Then, the TMD flakes were scrolled into NSs in just 5 s with a nearly 100% yield by placing one drop of ethanol solution (volume ratio of ethanol:water = 2:1) on their surface. Other aqueous solutions, such as methanol, tetrahydrofuran, dimethylformamide, and *N*-methyl-2-pyrrolidone, can also be used for TMD flakes scrolling (Supplementary Fig. 1, 2 and Supplementary Note 1). In addition, the scrolling proceeded well for TMD flakes grown on other substrates, such as Si₃N₄ and sapphire (Supplementary Fig. 3). To clarify the TMD-NSs formation process, the entire procedure was recorded using a CCD camera equipped on an optical-microscope (Supplementary Movie 1). A series of steps that might have led to the formation of the TMD-NSs are proposed in Fig. 1. Monolayer TMD flakes were grown on a substrate at a high temperature (≥ 720 °C). During the process of cooling down to room temperature, a strain was introduced to the TMD flakes because of the mismatch in thermal expansion coefficients between the TMD flake and the substrate. Stable TMD flakes were achieved when the strain and substrate adhesion were balanced. When an ethanol solution spread onto the surface of TMD flakes, the liquid film intercalated into the TMD flakes and the substrate, as demonstrated by the contrast color change in the flakes (Supplementary Fig. 4). With the liquid intercalation, part of the TMD flake was first released from the substrate to become freestanding as shown in Fig. 1. Under the built-in strain, the released part of the flake curved out of the plane and continued to roll up to a complete NS in the solution. An energy analysis of the MoS₂ flakes before and after scrolling was presented in the Supplementary Note 2. The energy barrier required to bend the freestanding flake out of plane was proved to be relatively low, indicating the easy nucleation of a scroll. In addition, the strain energy induced from the thermal mismatch of the MoS₂ flake was found high enough to activate the formation of scrolls after the liquid intercalation and the adhesion energy of the MoS₂ flake with substrate decreasing (Supplementary Fig. 5). Strain as the stimulus to the NSs

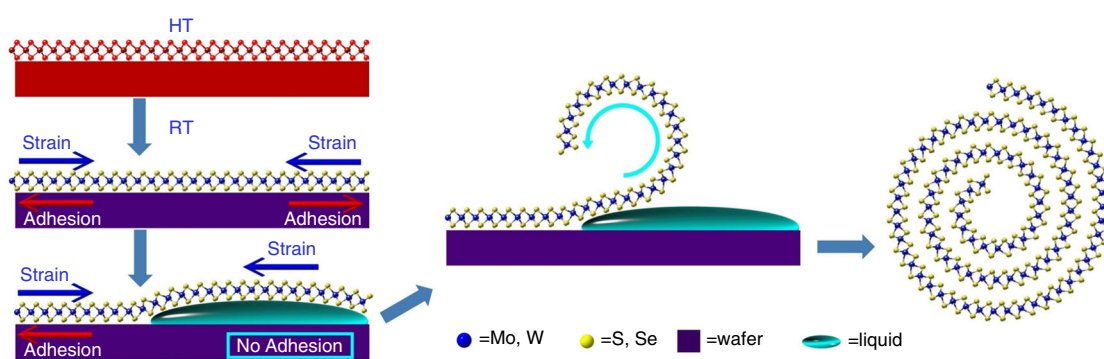


Fig. 1 Schematic of self-scrolling of chemical vapor deposition (CVD)-based transition metal dichalcogenide (TMD) monolayer flakes. A proposed series of steps leading to the formation of TMD-NSs is shown: (I) initial TMD monolayer growth on a substrate at a high temperature (HT) (e.g., 720, 825 °C); (II) the generation of a strain, balanced with the adhesion from substrate, in the TMD monolayer while cooling down to room temperature (RT); (III) the insertion of liquid between the TMD monolayer and substrate and the disappearance of the adhesion; (IV) the TMD flakes curve out of the plane driven by the strain; (V) the final formation of TMD-NSs

formation was also suggested by the following fact. When treated with ethanol solution, freshly produced TMD flakes on substrates were more prone to scroll in the shortest time with the highest yield, while the aged samples exhibited slightly decreased scrolling speed and yield. A few cracks were observed in aged samples by scanning electron microscopy (SEM, Supplementary Fig. 6), and these cracks could have partially relieved the strain.

TMD flakes were observed to prefer to scroll along one edge where the adhesion with the substrate was first relaxed upon the intercalation of the liquid. As the edges of CVD-grown TMD single crystals have a zigzag orientation^{4,22,23}, the chirality of their NSs are defined (Supplementary Fig. 7). For large-area polycrystalline films without regular edges, the orientation and chirality of their NSs are generally random (Fig. 2a, b). Thus, the controllable scrolling of TMD films was attempted (Fig. 2c–e and Supplementary Fig. 8). Using a focused ion beam (FIB), a MoS₂ polycrystalline film was patterned into parallel ribbons with defined width and direction (Fig. 2c) to produce long NS arrays (Fig. 2d). Using FIB etching a second time, long NSs were further arranged into periodic arrays with a controlled length (Fig. 2e). These NS arrays have promise for wide application, such as integrated circuits and matrix displays. We assume that horizontal TMD-NS arrays with controllable chirality could potentially be achieved by controlling the crystal orientation of the ribbon edges via etching from one large-area TMD single

crystal, which is prevented by the technique to synthesize large-area TMD single crystals.

Morphology characterization. CVD-grown TMD flakes are high quality even comparable to intrinsic flakes^{23,24}. The ethanol solution was clean and harmless; therefore, no defects or impurities were introduced into the high-quality TMD-NSs (Supplementary Fig. 9). Based on this method, several typical TMD-NSs, including those of MoS₂ (Fig. 2f and Supplementary Fig. 10), WS₂ (Fig. 2g), MoSe₂ (Fig. 2h), and WSe₂ (Fig. 2i), were successfully fabricated. Most of the NSs displayed a straight and compact appearance. High-resolution transmission electron microscopy (HR-TEM) was used to further examine the TMD-NSs microstructure, which was found to be multiwalled and tubular (Fig. 2j–m). The diameter and sidewall thickness of the TMD-NS varied with the size of the original flake. The hollow diameters were 10–40 nm. In addition, the high-magnification images of the sidewalls and the selected area electron diffraction (SAED) both showed that the TMD layers in the NSs were stacked uniformly and compactly (Fig. 2j–m inset and Supplementary Fig. 11). The distance between adjacent walls was approximately 6.21 Å, 6.41 Å, 6.35 Å, and 6.45 Å for MoS₂-, WS₂-, MoSe₂-, and WSe₂-NSs, respectively, which matched the interlayer spacing in bulk TMDs (6.15 Å, 6.36 Å, 6.45 Å, and 6.49 Å for MoS₂, WS₂, MoSe₂, and

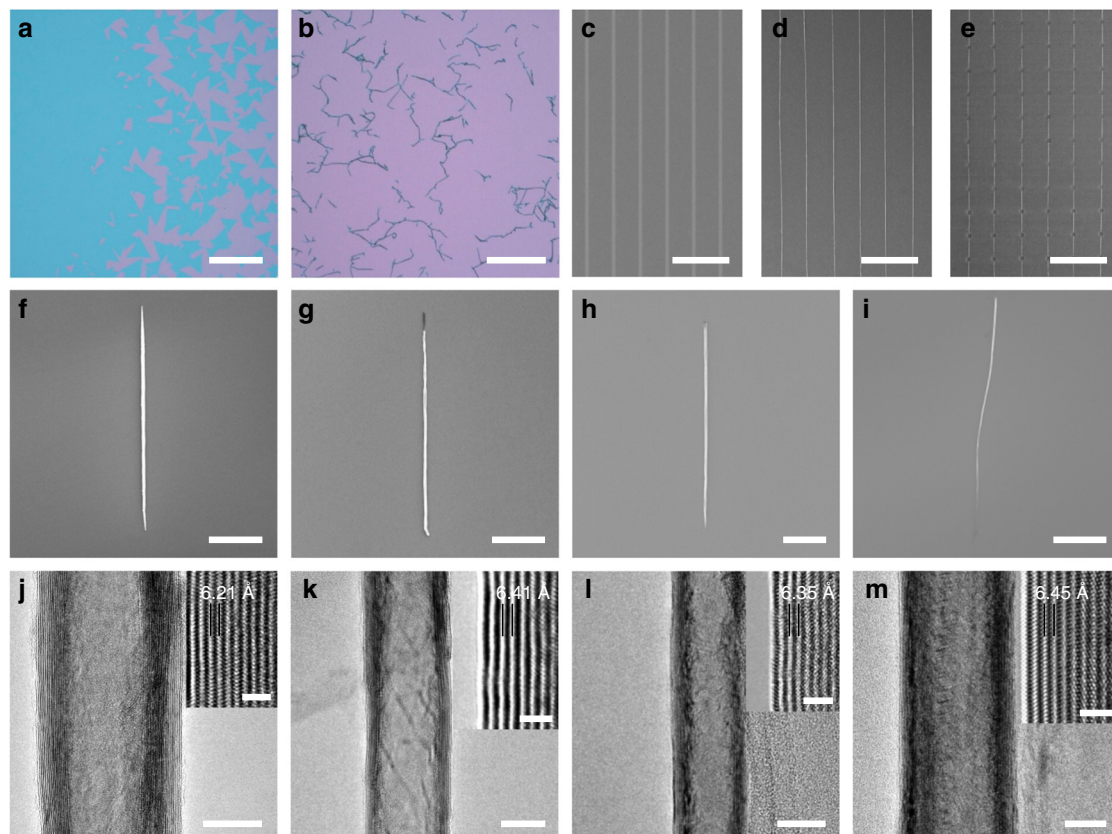


Fig. 2 Transition metal dichalcogenide (TMD)-nanoscrolls (NSs) from self-scrolling chemical vapor deposition (CVD)-based TMD monolayer flakes. **a** Optical image of CVD-grown MoS₂ monolayer flakes on a SiO₂/Si substrate (the purple area represents the substrate, the green area represents the MoS₂ monolayers; scale bar, 500 μm). **b** Optical image of MoS₂-NSs on a SiO₂/Si substrate (scale bar, 100 μm). **c–e** The fabrication process of a MoS₂-NS array (scanning electron microscopy—SEM image shown, scale bars, 50 μm). **c** Large-area MoS₂ monolayer film patterned into ribbons by focused ion beam (FIB) etching (the dark region represents MoS₂ film, the bright area is bare substrate). **d** Long MoS₂-NSs made from the controllable scrolling of the patterned MoS₂ film in **c**. (The white parallel lines are MoS₂-NSs, and the dark area represents the substrate). **e** A 12 × 6 array of MoS₂-NSs fabricated via a second FIB etching of the long MoS₂-NSs in **d**. **f–i** SEM images of typical TMD-NSs on SiO₂/Si substrates: MoS₂-NSs (**f**), WS₂-NSs (**g**), MoSe₂-NSs (**h**), and WSe₂-NSs (**i**). (Scale bars, 5 μm in **f**, **i** and 10 μm in **g**, **h**). **j–m** TEM images of typical TMD-NSs: MoS₂-NSs (**j**), WS₂-NSs (**k**), MoSe₂-NSs (**l**), and WSe₂-NSs (**m**). (Scale bars, 20 nm). Inset: High-magnification images of sidewalls of TMD-NSs (scale bars, 2 nm)

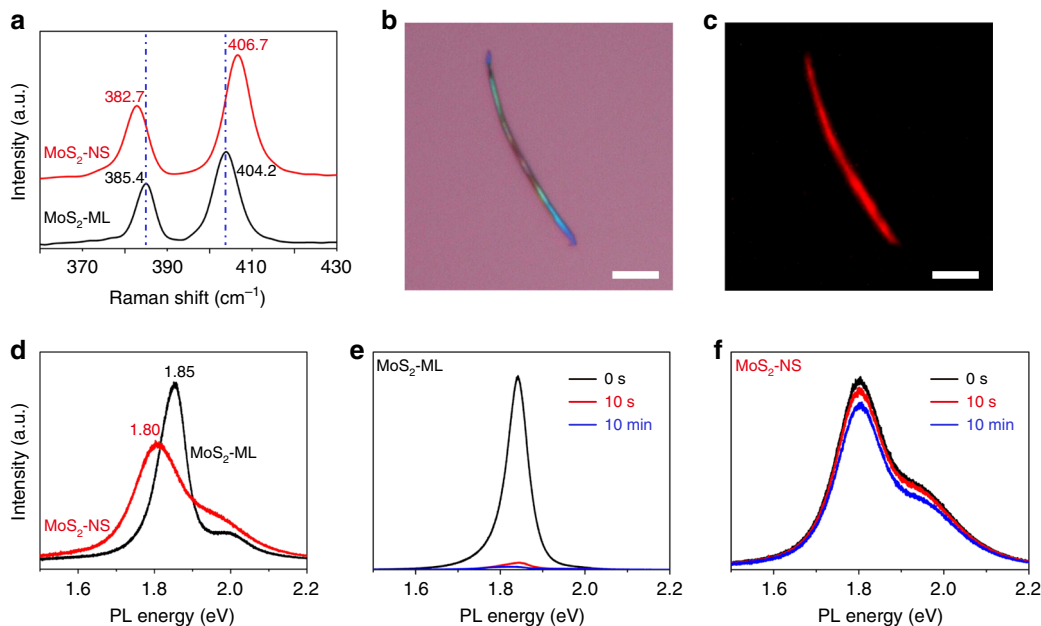


Fig. 3 Optical characterization of MoS₂-NSs (nanoscrolls). **a** Raman spectra of chemical vapor deposition (CVD)-grown MoS₂ monolayers (MoS₂-ML, black line) and MoS₂-NSs (red line) with 532 nm excitation. **b** Optical image of a typical MoS₂-NS. **c** Corresponding fluorescence image of the MoS₂-NS in **b**. The fluorescence image was obtained with an excitation wavelength of 510–560 nm. **d** PL spectra from MoS₂ monolayer (black line) and MoS₂-NSs (red line) (532 nm excitation). **e**, **f** PL spectra response of MoS₂ monolayer (**e**) and MoS₂-NSs (**f**) with NH₃ doping for 0 s (black line), 10 s (red line), and 10 min (blue line) (scale bars, 5 μm in **b** and **c**)

WSe₂, respectively), indicating both the tight scrolling of the TMD flakes and the lack of interlayer contamination.

Optical characterization. Raman spectra of the TMD-NSs were recorded using 532 nm excitation (Fig. 3a and Supplementary Fig. 12a–c). The Raman signature of monolayer MoS₂ flakes is consistent with that of mechanically exfoliated monolayer MoS₂²⁵. A similar Raman signature was also found for MoS₂-NSs, demonstrating the good crystallinity of the MoS₂-NSs. A blue shift was observed in the A_{1g} mode from 404.2 cm⁻¹ for the monolayer MoS₂ to 406.7 cm⁻¹ for the MoS₂-NSs, and this shift was attributed to the van der Waals interactions between neighboring NS layers^{25,26}. Additionally, a red shift in the E_{2g} mode was detected from 385.4 cm⁻¹ for the monolayer MoS₂ to 382.7 cm⁻¹ for the MoS₂-NSs, resulting from stacking-induced structural changes, long-range Coulombic interlayer interactions^{25,27}, or/and a slight tension owing to the bending deformation of the flake²⁸. The frequency shift behavior reflects structural changes after scrolling, and the changes were also observed for WS₂-, MoSe₂-, and WSe₂-NSs (Supplementary Fig. 12a–c).

Semiconducting TMD monolayers are direct-bandgap materials because of quantum confinement effects²⁹. The strong photoluminescence (PL) and a wide range of band gaps of the monolayer TMD semiconductors indicate their potential for use in 2D optoelectronics, such as optical energy conversion devices³⁰ or photodetectors³¹. Despite having a stacking structure similar to that of bulk TMDs, these TMD-NSs were shown to have an obvious PL, in contrast with the bulk counterparts, in which PL is negligible²⁹. Red luminescence from a typical MoS₂-NS was clearly observed by fluorescence imaging, indicating that the PL was sufficiently strong to be imaged (Fig. 3b, c). In the PL spectra of Fig. 3d, A, B direct excitonic transitions²⁹ from MoS₂-NSs appeared at around 1.80 eV (688 nm) and 1.95 eV (635 nm), matching their absorption resonances (Supplementary Fig. 13). Compared with monolayer MoS₂, a red shift in the A exciton transition, approximately of

30–60 meV was found for MoS₂-NSs and was accompanied by an increase in the full-width at half-maximum of 50–80 meV. The red shift of A peak, an indicator of the variation of the electronic structure, can be explained by the stacking and tension effects in the NSs^{29,32,33}, while PL peak broadening is presumably owing to the overlap of signals from several MoS₂ layers in a NS. Analogous PL behavior was also observed for the WS₂-, MoSe₂-, and WSe₂-NSs (Supplementary Fig. 12d–f).

It is well known that monolayer TMD atoms are fully exposed, which makes their optical and electrical properties sensitive to environmental factors. As shown in Fig. 3e, f, when exposed to NH₃, the PL intensity of monolayer MoS₂ flakes was quenched rapidly and drastically; in contrast, the PL intensity of MoS₂-NSs did not show a pronounced decrease. Apparently, the optical properties of MoS₂-NSs were less dependent on the environment, which might be attributed to the self-encapsulated structure, where most of the MoS₂ flakes were rolled up inside and sealed by the outermost layers.

FET performance. Since TMD-NSs are semiconductors, and there are no previous reports on their FET properties, it is interesting to explore this issue here. Device characterization is easy for MoS₂-NSs because the NSs have been produced on a SiO₂/Si substrate. Defining source and drain electrodes were directly deposited on the top of MoS₂-NSs via a shadow mask. This process avoided organic impurity contamination that might occur during traditional electron-beam lithography. The FETs based on the MoS₂-NSs exhibited good FET behavior, and the current/voltage characteristics conformed well to conventional transistor models in both saturated and linear regimes in N₂ (Fig. 4 and Supplementary Fig. 14). According to the equation below, we calculated the mobility in the saturation regime.

$$I_D = (W/2L)C_i\mu(V_G - V_T)^2,$$

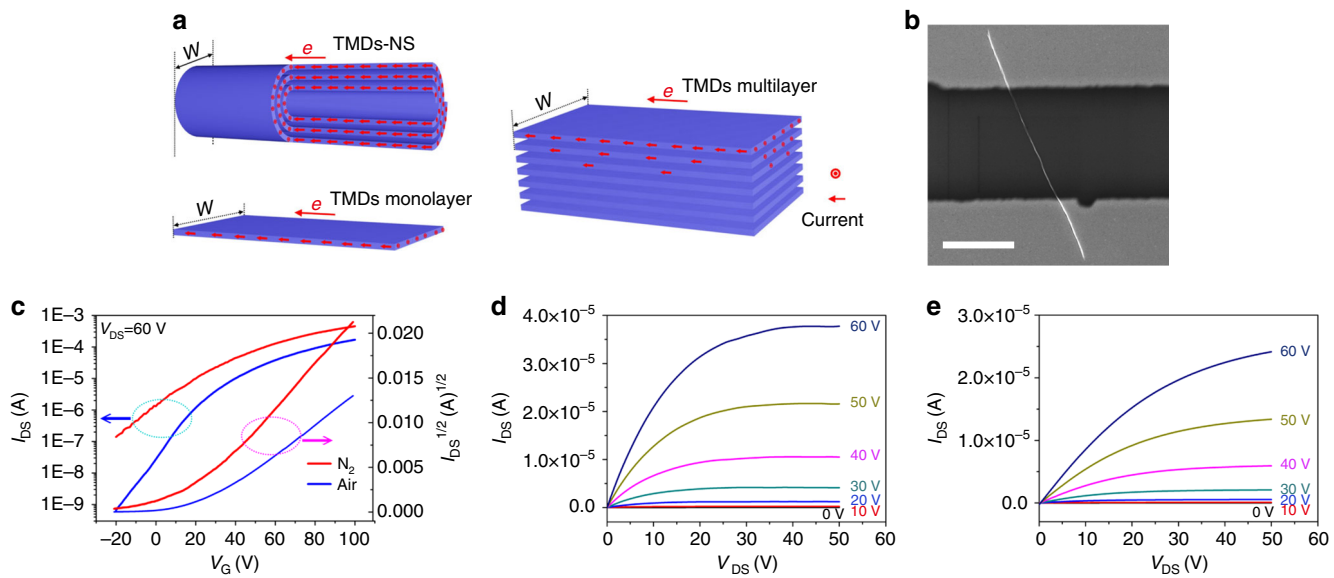


Fig. 4 Electrical characteristics of MoS₂-NSs (nanoscrolls). **a**, Schematic representations of current conduction in transition metal dichalcogenide (TMD)-nanoscrolls (NSs), TMDs monolayer, and TMDs multilayer under bias. The W represents the conduction channel width. The NSs made from the below TMDs monolayer have a much shorter W . For TMDs multilayer, the current only passes through the outermost shell layers. **b**, SEM image of a typical MoS₂-NS FET (scale bar, 10 μ m). **c**, Transfer characteristics of MoS₂-NS tested in N₂ (red) and air (blue). **d**, Output characteristics of MoS₂-NS tested in N₂. **e**, Output characteristics of MoS₂-NS tested in air

where L and W are the channel length and width, respectively, C_i is the insulator capacitance per unit area (11 nF cm⁻²), μ is the FET mobility, and V_T is the extrapolated threshold voltage. More than 300 devices were tested. The electron mobility of NSs was measured to be mostly in the range 200–700 cm² V⁻¹ s⁻¹, with an on/off ratio of over 1.0×10^5 . The mobility of MoS₂-NSs, nearly 30-fold greater than that of monolayer MoS₂ flakes (10–20 cm² V⁻¹ s⁻¹)³⁴, should be ascribed to the high current density for compact scroll topology. Invoking an Archimedean spiral model, we quantified the change in the conduction channel widths upon scroll (the detailed analysis is provided in Supplementary Note 3). A considerable reduction in conduction channel widths was achieved after scrolling, while there is no significant decline in the current for the flakes upon scrolling process (Supplementary Fig. 15, 16). This led to a higher current density and mobility. In addition, benefiting from the compact scrolling, conductive layers in a NS compactly stacked layer by layer. The adjacent layers acted as ideal substrates for each other with atomically smooth surface, relatively no dangling bonds and charge traps, which also enhanced electron transporting efficiency³⁵. With the similar stacked layer structures, however, the MoS₂-NSs also exhibited much greater electron mobility than did the multilayer MoS₂ flakes³⁶. It can be explained that in a MoS₂-NS, electrons are transported through the whole scrolled MoS₂ flake, while in multilayer MoS₂ flakes, electrons are blocked by van der Waals gaps while migrating to inner layers; thus, only a few shell layers contribute to the carriers transmission (Fig. 4a). The monolayer MoS₂-based FETs were observed to be very sensitive to atmosphere. However, there was no obvious decrease in FET mobility for the MoS₂-NSs when they were tested in air (Fig. 4c–e)

because most of each electrically active MoS₂ layers is encapsulated within each NS and the compact stacked (with an interlayer distance of 0.62 nm) morphology can efficiently prevent oxygen from intercalating into the MoS₂-NSs to deteriorate transistors performance. The high mobility and unique self-encapsulated morphology make MoS₂-NSs promising in FETs.

Hybrid TMD-NSs. As mentioned above, TMD-NSs are inert to the outside owing to their self-encapsulated structures; however, they are inclined to be doped and form composites because of their internal open topological structures. With a pretreatment, TMD flakes can be hybridized with diverse loads, which become sandwiched into the van der Waals gaps upon flakes scrolling (Fig. 5a). In this paper, we produced MoS₂-NSs hybridized with gold nanoparticles (AuNPs) (Fig. 5b), graphene oxide (GO) (Fig. 5c), pentacene (Fig. 5d), copper (II) phthalocyanine (CuPc) (Fig. 5e), poly{2,2'-(2,5-bis(2-hexyldecyl)-3,6-dioxo-2,3,5,6-tetrahydropyrrolo[3,4-c]pyrrole-1,4-diyl)dithiophene}-5,5'-diyl-alt-thiophen-2,5-diyl} (PDPP3T) (Fig. 5f), DNA (Fig. 5g) and polypeptide (Fig. 5h). In contrast with nanotubes, the lattice spacing of NSs can adjust automatically upon hybridization with foreign substances of different sizes, and this adjustment can be evaluated by HR-TEM. Figure 5b–h displayed the lattice spacing of hybrid NSs, where lattice expansion was observed for all composite NSs, and some composite components, such as AuNPs, were large enough to be directly visualized (Fig. 5b). Moreover, Raman spectroscopy was utilized to verify the presence of foreign substances. As a typical example, the intercalation of GO into NSs was verified by the emergence of the D, G, and 2D peaks of GO (around 1350, 1600, 2671 cm⁻¹)³⁷, as well as vibrational modes (around 383, 406 cm⁻¹) for MoS₂ (Supplementary Fig. 17a). In addition, TMD-NSs can be conferred with additional properties and functions upon hybridization with other functional materials, such as organic small molecules, polymers, nanoparticles, and 2D materials, as well as biological substances. For example, after hybridization with PDPP3T, a new fluorescence peak appeared at about 1.42 eV (873 nm) for MoS₂-NSs (Supplementary Fig. 17b), indicating that the hybridization broadened MoS₂-NS emission spectrum and could eventually extend their optical applications. Furthermore, the intercalated NS by PDPP3T exhibited a good stability in air, due to the self-encapsulated structure (Supplementary Fig. 18).

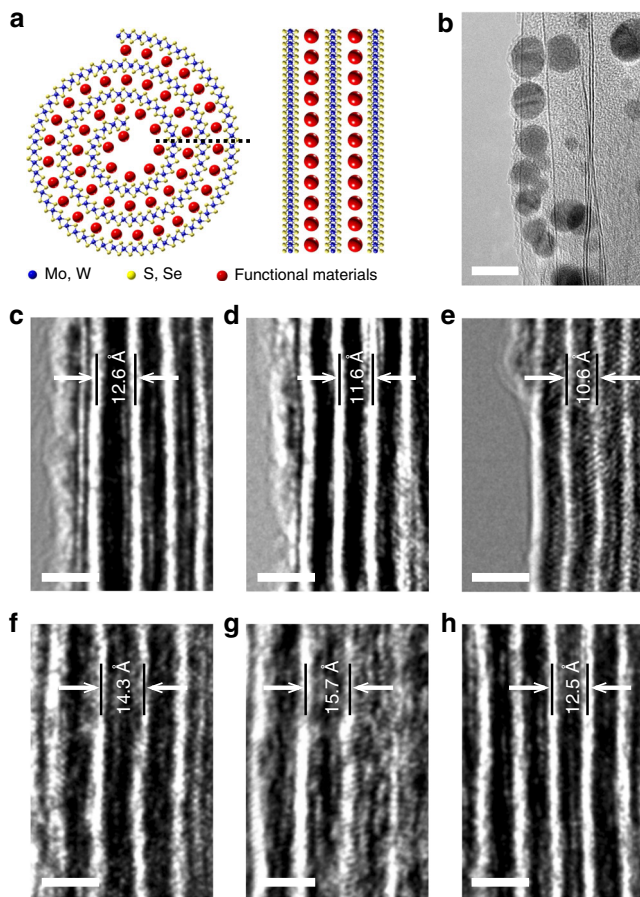


Fig. 5 Hybrid transition metal dichalcogenide (TMD)-nanoscrolls (NSs). **a**, Schematic showing the cross section and sidewalls of hybrid TMD-NSs. **b–h**, HR-TEM images of sidewalls of MoS₂-NSs hybridized with AuNPs (**b**), GO (**c**), pentacene (**d**), CuPc (**e**), PDPP3T (**f**), DNA (**g**) and polypeptide (**h**). AuNPs approximately 5 nm in diameter were clearly observed between the walls; the GO flakes were also distinguishable, as shown in **c**. Lattice expansion was displayed in all hybrid NSs above. The bright white walls represent the MoS₂ layers in (**c–h**) (scale bars, 10 nm in **b** and 2 nm in **c–h**).

Discussion

In summary, we have explored a simple method for producing high-quality, tightly scrolled TMD-NSs from CVD-grown monolayer TMD flakes with the assistance of one drop of an ethanol solution. An obvious PL was shown in TMD-NSs, with a red shift in the direct excitonic transitions. The electron mobility of the MoS₂-NSs was approximately 30-fold greater than that of the monolayer MoS₂ flakes. This scrolling strategy will be a candidate for increasing mobility of other 2D materials. Owing to their unique self-encapsulated structures, these TMD-NSs show stable optical and electronic properties in different atmospheres. The HR-TEM results show the internal open topological structure of the TMD-NSs, which serve as effective carriers for accommodating external substance of different sizes in their tunable van der Waals gaps. The hybridization with other functional materials will confer TMD-NSs with additional properties and functions attractive for potential application.

Methods

CVD growth of TMD monolayers. TMD monolayers were grown by an atmospheric pressure CVD. The growth substrates, including SiO₂/Si, Si₃N₄ and sapphire, were cleaned in acetone, isopropanol, and deionized water and then dried under high-purity nitrogen flow.

For MoS₂ monolayers, the growth substrate was placed face-down above a ceramic boat containing MoO₃ powder (Sigma Aldrich, 99.998%, 20 mg). The ceramic boat was then loaded in the heating zone center of the furnace tube, where another boat containing 80 mg of sulfur (Alfa Aesar, 99.999%) was located upstream. The tube was first purged with ultrahigh-purity argon for 10 min at a flow rate of 200 sccm. Then, the furnace was heated from room temperature to 500 °C in 12 min, 500–720 °C in another 20 min, and then stayed at 720 °C for 5 min. The sulfur was heated to 130 °C with a separate heat setup as the furnace reached 720 °C. Finally, the temperature was cooled from 720 to 570 °C in 20 min before opening the furnace for rapid cooling. Argon as carrier gas was maintained at a flow rate of 10 sccm throughout the growth process.

The growth of WS₂ monolayers was similar to that of MoS₂, except that WO₃ (Alfa Aesar, 99.998%, 10 mg) was used as one of the precursors and the highest growth temperature was set at 825 °C, with sulfur at 150 °C.

WSe₂ monolayers were grown on substrates with WO₃ (10 mg) and selenium powders (Alfa Aesar, 99.999% + %, 1–5 mm) as precursors. The growth recipe was as follows: ramp the furnace from room temperature to 825 °C in 20 min, sit 20 min at 825 °C, cool to 600 °C in 20 min, and open the furnace for rapid cooling. The selenium powders were heated to 300 °C when the furnace temperature rose to 825 °C and were maintained at this temperature for 40 min. 1.5 sccm hydrogen and 23.5 sccm argon were used during the growth process.

MoSe₂ monolayers were grown via procedure similar to that used for WSe₂ monolayers, except that the source precursors were MoO₃ and selenium, and the selenium was kept at 400 °C during the growth process.

Fabrication of TMD-NSs. TMD-NSs were fabricated by dropping an ethanol aqueous solution onto the CVD-grown TMD monolayers and allowing it to dry naturally. Rod-like NSs were then obtained on the substrate. The concentration of the ethanol aqueous solution ranged from 5:1 to 1:1 (volume ratio of ethanol:water), with an optimum ratio of 2:1.

MoS₂-NSs arrays. A MoS₂ polycrystalline film was first patterned into parallel ribbons with defined width and direction using a FIB. A drop of pure ethanol was dropped on the patterned film, and then a coverslip was put on top of it. A thin liquid layer of pure ethanol can be formed between the film and the coverslip. An ethanol solution (1:1) was then dropped on the edge of the coverslip. Drove by the concentration gradient, the water in the solution will slowly infiltrate into the pure ethanol under the coverslip in the gradient direction (as shown in Supplementary Fig. 8). The diffusion rate can be adjusted by the concentration of the ethanol solution. In this way one side of a ribbon was first controlled to scroll to produce a long NS. The long NS array was then fabricated and further arranged into periodic arrays with a controlled length by FIB etching a second time.

Hybrid MoS₂-NSs fabrication. Pentacene/MoS₂-NSs: a 1-nm-thick layer of pentacene was deposited on the MoS₂ monolayers on a SiO₂/Si substrate by vacuum thermal evaporation, followed by immersion into a modulated ethanol solution (5:1). After 10 min, the substrate was picked up and allowed to dry naturally. The pentacene/MoS₂-NSs were obtained. The CuPc/MoS₂-NSs were prepared in the same way.

PDPP3T/MoS₂-NSs: A PDPP3T solution was prepared by dissolving 2 mg of PDPP3T powder in 1 ml of toluene. After stirring overnight, the PDPP3T solution was spin-coated onto the MoS₂ monolayers at a speed of 5000 rpm. After annealing at 70 °C for 20 min, the PDPP3T-coated MoS₂ monolayers were then dipped into an ethanol solution (5:1). After 10 min, the MoS₂ monolayers were picked up and dried naturally.

GO/MoS₂-NSs: This procedure is similar to that used for PDPP3T/MoS₂-NSs. Freshly exfoliated GO sheets were dispersed in *n*-hexane and then spin-coated onto MoS₂ monolayers. After dropping an ethanol solution (2:1) onto the samples, the GO/MoS₂-NSs were obtained.

Au/MoS₂-NSs: MoS₂ monolayers were dipped into an ethanol solution (2:1) containing AuNPs. Ten minutes later, the MoS₂ monolayers were picked up and dried naturally. Similar procedures were used for producing both DNA/MoS₂- and polypeptide/MoS₂-NSs.

MoS₂-NS-based FET. Freshly made monolayer MoS₂ flakes on a SiO₂/Si substrate were kept in nitrogen for 48 h. Then the MoS₂ flakes were scrolled into NSs with one drop of ethanol solution (2:1) in nitrogen atmosphere. Bottom-gated transistors based on these MoS₂-NSs were fabricated on the SiO₂/Si substrate without additional transfer. 100 nm of Au was deposited on the top of MoS₂-NSs as source and drain electrodes with a shadow mask by vacuum thermal evaporation at a rate of about 0.3 Å s⁻¹. The electrical measurements were conducted under a nitrogen atmosphere and ambient condition, respectively.

Characterization. Raman and PL measurements were performed with a 532 nm laser under ambient conditions (inVia-Reflex). All optical images and the video were captured with a Nikon Eclipse LV100D. The fluorescence microscope characterization was performed using a fluorescence microscope equipped with a mercury lamp as the excitation light source. Large-area MoS₂ films and long MoS₂-NSs were etched via FIB-SEM (FEI, Helios Nanolab G3 CX). SEM

(Hitachi S-4800) and HR-TEM (JEOL JEM-2100F) were employed to image the samples. Current-voltage curves were obtained by a three-probe station under a nitrogen atmosphere and ambient conditions (Keithley 4200 SCS).

Data availability. The data that support the findings of this study are available from the corresponding author on reasonable request.

Received: 24 August 2017 Accepted: 8 March 2018

Published online: 03 April 2018

References

- Wang, Q. H., Kalantar-Zadeh, K., Kis, A., Coleman, J. N. & Strano, M. S. Electronics and optoelectronics of two-dimensional transition metal dichalcogenides. *Nat. Nanotechnol.* **7**, 699–712 (2012).
- Chhowalla, M. et al. The chemistry of two-dimensional layered transition metal dichalcogenide nanosheets. *Nat. Chem.* **5**, 263–275 (2013).
- Kang, K. et al. High-mobility three-atom-thick semiconducting films with wafer-scale homogeneity. *Nature* **520**, 656–660 (2015).
- Chen, J. et al. Chemical vapor deposition of large-size monolayer MoSe₂ crystals on molten glass. *J. Am. Chem. Soc.* **139**, 1073–1076 (2017).
- Gong, Y. et al. Vertical and in-plane heterostructures from WS₂/MoS₂ monolayers. *Nat. Mater.* **13**, 1135–1142 (2014).
- Duan, X. et al. Lateral epitaxial growth of two-dimensional layered semiconductor heterojunctions. *Nat. Nanotechnol.* **9**, 1024–1030 (2014).
- Li, M. Y. et al. Epitaxial growth of a monolayer WSe₂-MoS₂ lateral pn junction with an atomically sharp interface. *Science* **349**, 524–528 (2015).
- Li, X. et al. Two-dimensional GaSe/MoSe₂ misfit bilayer heterojunctions by van der Waals epitaxy. *Sci. Adv.* **2**, e1501882 (2016).
- Pan, H., Feng, Y. & Lin, J. Ab initio study of electronic and optical properties of multiwall carbon nanotube structures made up of a single rolled-up graphite sheet. *Phys. Rev. B* **72**, 085415 (2005).
- Chen, Y., Lu, J. & Gao, Z. Structural and electronic study of nanoscrolls rolled up by a single graphene sheet. *J. Phys. Chem. C* **111**, 1625–1630 (2007).
- Chang, C. & Ortix, C. Theoretical prediction of a giant anisotropic magnetoresistance in carbon nanoscrolls. *Nano Lett.* **17**, 3076–3080 (2017).
- Liu, Z., Gao, J., Zhang, G., Cheng, Y. & Zhang, Y. From two-dimensional nano-sheets to roll-up structures: expanding the family of nanoscroll. *Nanotechnology* **28**, 385704 (2017).
- Zheng, J. et al. Production of high-quality carbon nanoscrolls with microwave spark assistance in liquid nitrogen. *Adv. Mater.* **23**, 2460–2463 (2011).
- Zheng, B., Xu, Z. & Gao, C. Mass production of graphene nanoscrolls and their application in high rate performance supercapacitors. *Nanoscale* **8**, 1413–1420 (2016).
- Berman, D., Deshmukh, S. A., Sankaranarayanan, S. K. R. S., Erdemir, A. & Sumant, A. V. Macroscale superlubricity enabled by graphene nanoscroll formation. *Science* **348**, 1118–1122 (2015).
- Xie, X. et al. Controlled fabrication of high-quality carbon nanoscrolls from monolayer graphene. *Nano Lett.* **9**, 2565–2570 (2009).
- Mpourmpakis, G., Tylianakis, E. & Froudakis, G. E. Carbon nanoscrolls: a promising material for hydrogen storage. *Nano Lett.* **7**, 1893–1897 (2007).
- Shi, X., Cheng, Y., Pugno, N. M. & Gao, H. A translational nanoactuator based on carbon nanoscrolls on substrates. *Appl. Phys. Lett.* **96**, 053115 (2010).
- Chen, X., Boulos, R. A., Dobson, J. F. & Raston, C. L. Shear induced formation of carbon and boron nitride nano-scrolls. *Nanoscale* **5**, 498–502 (2013).
- Thangasamy, P. & Sathish, M. Rapid, one-pot synthesis of luminescent MoS₂ nanoscrolls using supercritical fluid processing. *J. Mater. Chem. C* **4**, 1165–1169 (2016).
- Meng, J. et al. Rolling up a monolayer MoS₂ sheet. *Small* **12**, 3770–3774 (2016).
- Gutiérrez, H. R. et al. Extraordinary room-temperature photoluminescence in triangular WS₂ monolayers. *Nano Lett.* **13**, 3447–3454 (2012).
- Van Der Zande, A. M. et al. Grains and grain boundaries in highly crystalline monolayer molybdenum disulfide. *Nat. Mater.* **12**, 554–561 (2013).
- Chen, J. et al. Chemical vapor deposition of large-sized hexagonal WSe₂ crystals on dielectric substrates. *Adv. Mater.* **27**, 6722–6727 (2015).
- Lee, C. et al. Anomalous lattice vibrations of single-and few-layer MoS₂. *ACS Nano* **4**, 2695–2700 (2010).
- Li, H. et al. From bulk to monolayer MoS₂: evolution of Raman scattering. *Adv. Funct. Mater.* **22**, 1385–1390 (2012).
- Wieting, T. J. & Verble, J. L. Interlayer bonding and the lattice vibrations of β-GaSe. *Phys. Rev. B* **5**, 1473–1479 (1972).
- Rice, C. et al. Raman-scattering measurements and first-principles calculations of strain-induced phonon shifts in monolayer MoS₂. *Phys. Rev. B* **87**, 081307 (2013).
- Mak, K. F., Lee, C., Hone, J., Shan, J. & Heinz, T. F. Atomically thin MoS₂: a new direct-gap semiconductor. *Phys. Rev. Lett.* **105**, 136805 (2010).
- Britnell, L. et al. Strong light-matter interactions in heterostructures of atomically thin films. *Science* **340**, 1311–1314 (2013).
- Lopez-Sanchez, O., Lembeck, D., Kayci, M., Radenovic, A. & Kis, A. Ultrasensitive photodetectors based on monolayer MoS₂. *Nat. Nanotechnol.* **8**, 497–501 (2013).
- He, K., Poole, C., Mak, K. F. & Shan, J. Experimental demonstration of continuous electronic structure tuning via strain in atomically thin MoS₂. *Nano Lett.* **13**, 2931–2936 (2013).
- Seifert, G., Terrones, H., Terrones, M., Jungnickel, G. & Frauenheim, T. Structure and electronic properties of MoS₂ nanotubes. *Phys. Rev. Lett.* **85**, 146 (2000).
- Najmaei, S. et al. Vapour phase growth and grain boundary structure of molybdenum disulphide atomic layers. *Nat. Mater.* **12**, 754–759 (2013).
- Fu, D. et al. Molecular beam epitaxy of highly crystalline monolayer molybdenum disulfide on hexagonal boron nitride. *J. Am. Chem. Soc.* **139**, 9392–9400 (2017).
- Kim, S. et al. High-mobility and low-power thin-film transistors based on multilayer MoS₂ crystals. *Nat. Commun.* **3**, 1011 (2012).
- Gao, L. et al. Face-to-face transfer of wafer-scale graphene films. *Nature* **505**, 190–194 (2014).

Acknowledgements

We thank Bo Guan and Xiang Li for the assistance with FIB-SEM. We thank Bo Guan for the assistance in SAED analysis. This work was supported by the Strategic Priority Research Programme of the National Natural Science Foundation (21573253), and the Chinese Academy of Sciences (XDB12010000).

Author contributions

X.C. performed the experiments, analyzed the data, and wrote the paper. J.Z. designed the work, performed the experiments, conceptualized the work, and analyzed the data. Z.K., D.H., Y.H., H.S., C.D., and D.Z. performed some characterization experiments and analyzed data. E.G. and Z.X. performed the theoretical analysis.

Additional information

Supplementary Information accompanies this paper at <https://doi.org/10.1038/s41467-018-03752-5>.

Competing interests: The authors declare no competing interests.

Reprints and permission information is available online at <http://npg.nature.com/reprintsandpermissions/>

Publisher's note: Springer Nature remains neutral with regard to jurisdictional claims in published maps and institutional affiliations.



Open Access This article is licensed under a Creative Commons Attribution 4.0 International License, which permits use, sharing, adaptation, distribution and reproduction in any medium or format, as long as you give appropriate credit to the original author(s) and the source, provide a link to the Creative Commons license, and indicate if changes were made. The images or other third party material in this article are included in the article's Creative Commons license, unless indicated otherwise in a credit line to the material. If material is not included in the article's Creative Commons license and your intended use is not permitted by statutory regulation or exceeds the permitted use, you will need to obtain permission directly from the copyright holder. To view a copy of this license, visit <http://creativecommons.org/licenses/by/4.0/>.

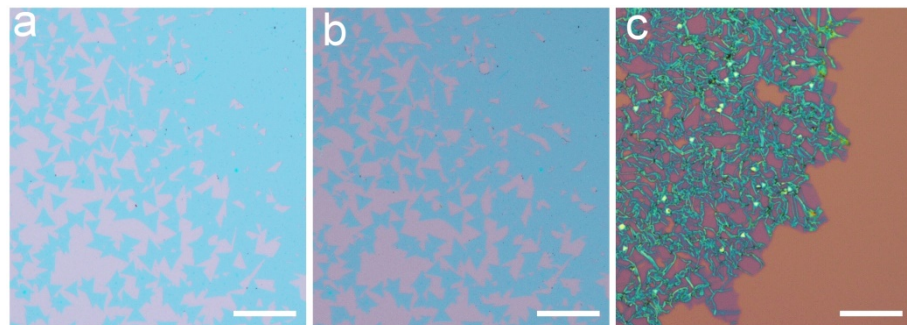
© The Author(s) 2018

Supplementary Information

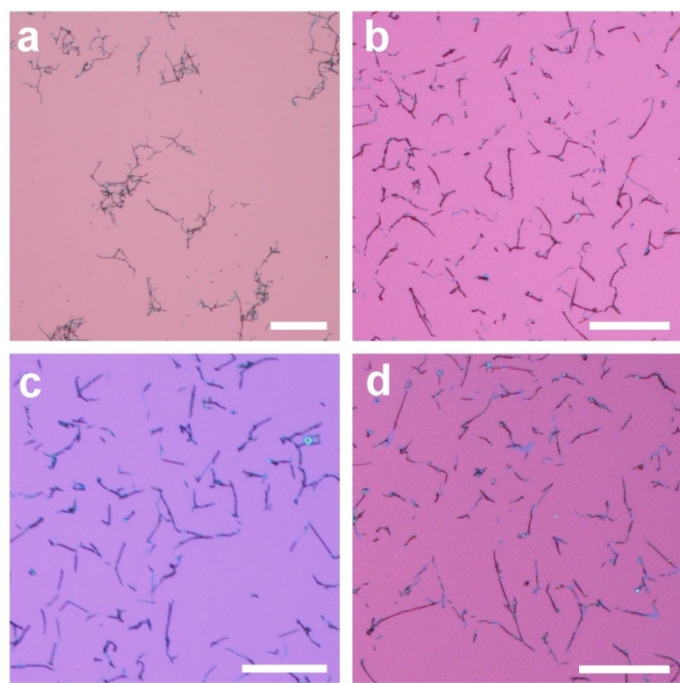
Rolling up Transition Metal Dichalcogenide Nanoscrolls via One Drop of Ethanol

Xueping Cui, Zhizhi Kong, Enlai Gao, Dazhen Huang, Yang Hao, Hongguang Shen,
Chong-an Di, Zhiping Xu, Jian Zheng^{*}, Daoben Zhu

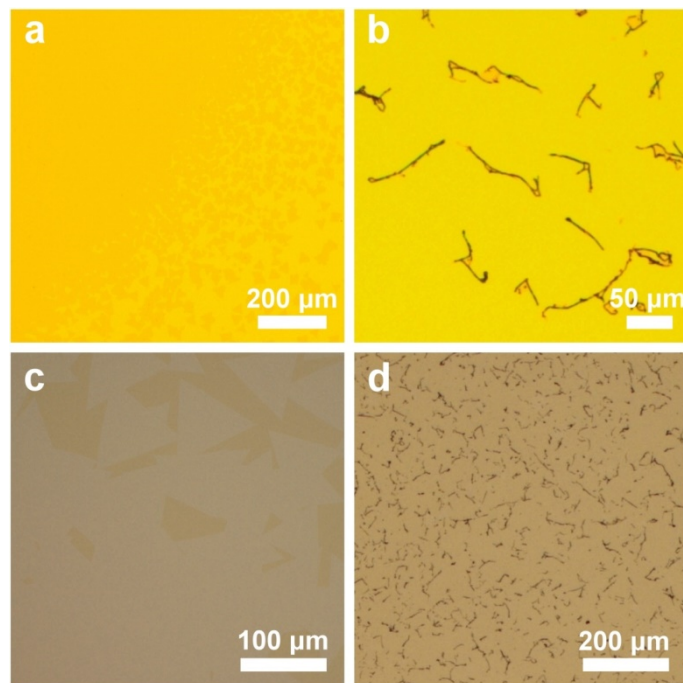
Supplementary Figures



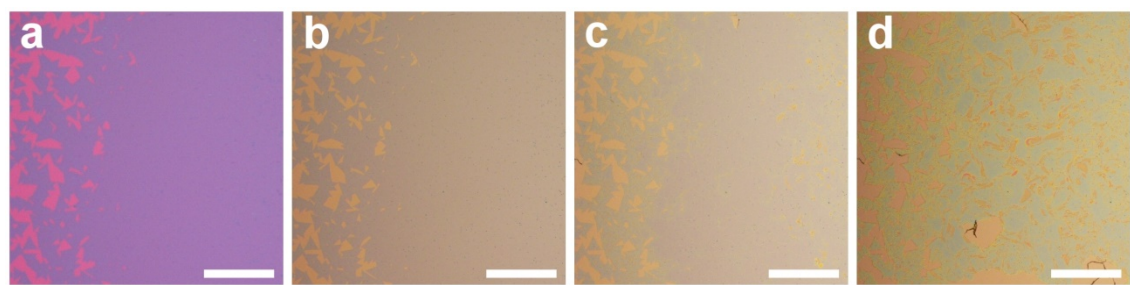
Supplementary Figure 1. **a**, Optical image of built-in tension released monolayer MoS₂ after transferred from growth substrate to another bare substrate. **b**, Optical image of the transferred sample after immersing into the ethanol solution. Almost no scroll was observed in the built-in tension released sample. **c**, Optical image of the MoS₂ sample after sharp intercalation of pure water. Loosely curled and disordered nanoscrolls with large unscrolled film were observed. (Scale bars, 200 μm in **a**, **b** and 20 μm in **c**).



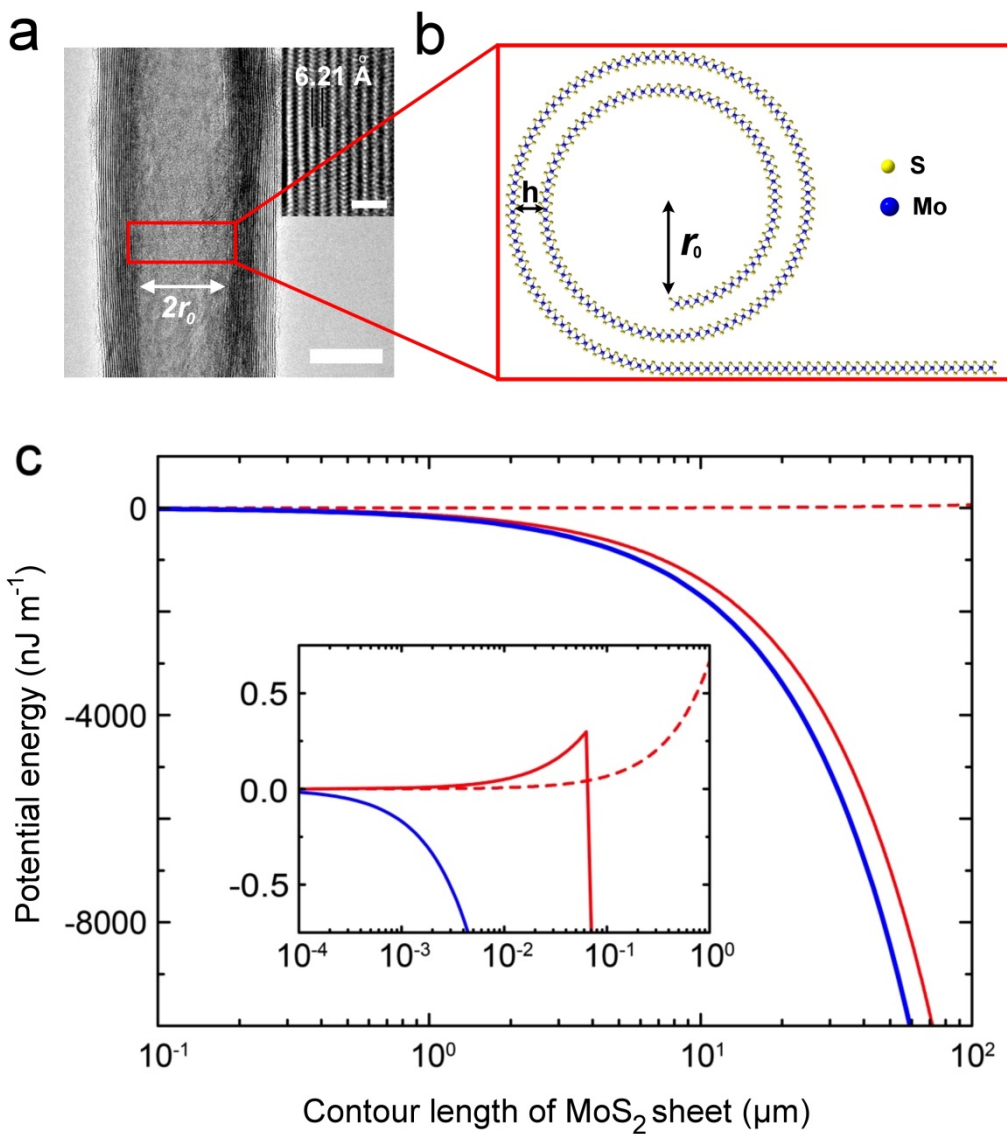
Supplementary Figure 2. MoS_2 -NSs made in the aqueous solution of methanol (**a**), tetrahydrofuran (**b**), dimethylformamide (**c**), and N-methyl-2-pyrrolidone (**d**). (Scale bars, 100 μm in **a** and 50 μm in **b-d**). Tight, straight scrolling with high yield can also be obtained with different solutions at the optimized ratio.



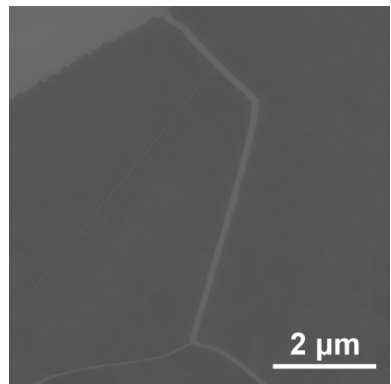
Supplementary Figure 3. MoS₂-NSs made from monolayer MoS₂ flakes grown on non-silicon substrates. **a**, Optical image of MoS₂ monolayers grown on a Si₃N₄ substrate. The dark yellow represents MoS₂ monolayers, and the light yellow is the Si₃N₄ substrate. **b**, Optical image of MoS₂-NSs made from MoS₂ monolayers grown on the Si₃N₄ substrate. **c**, Optical image of MoS₂ monolayers grown on a sapphire substrate. The white area represents MoS₂ monolayers, and the brown area represents the sapphire substrate. **d**, Optical image of MoS₂-NSs rolled up from MoS₂ monolayers grown on the sapphire substrate.



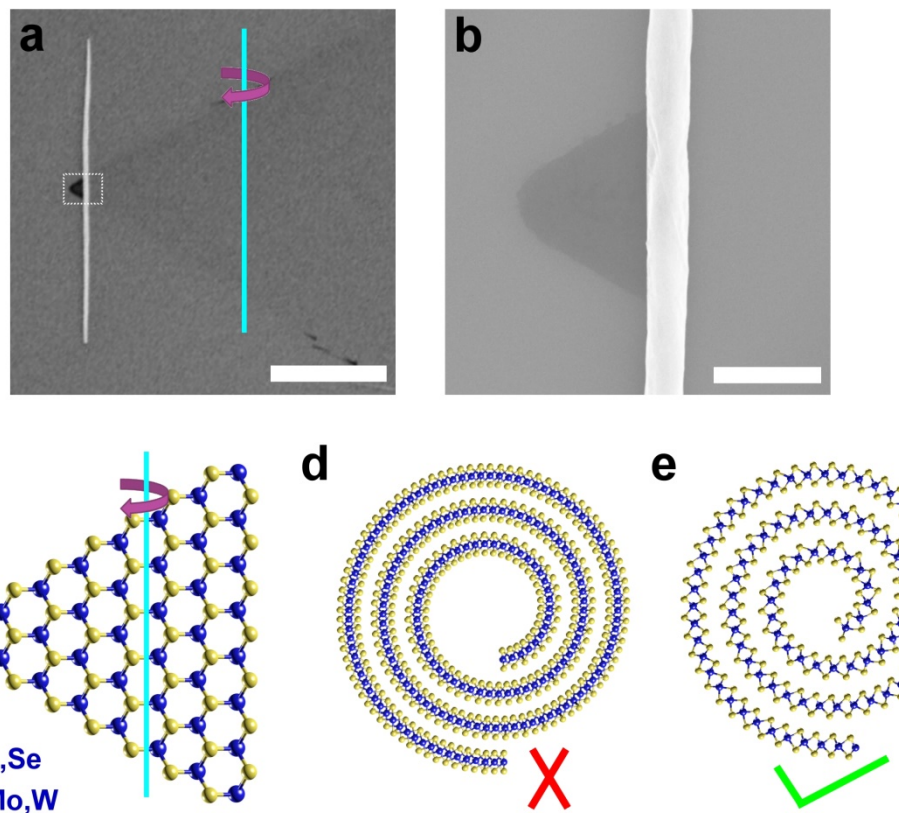
Supplementary Figure 4. The evolution in contrast color of MoS₂ flakes when treated by ethanol solution. **a**, Optical image of MoS₂ flakes on a SiO₂/Si substrate before dropping an ethanol solution. **b**, Optical image of MoS₂ flakes just covered with the ethanol solution. **c**, Optical image of MoS₂ flakes when a small amount of ethanol solution intercalating into MoS₂ flakes and the substrate **d**, Optical image of MoS₂ flakes when a large amount of ethanol solution intercalating into MoS₂ flakes and the substrate. (Scale bars, 100 μ m).



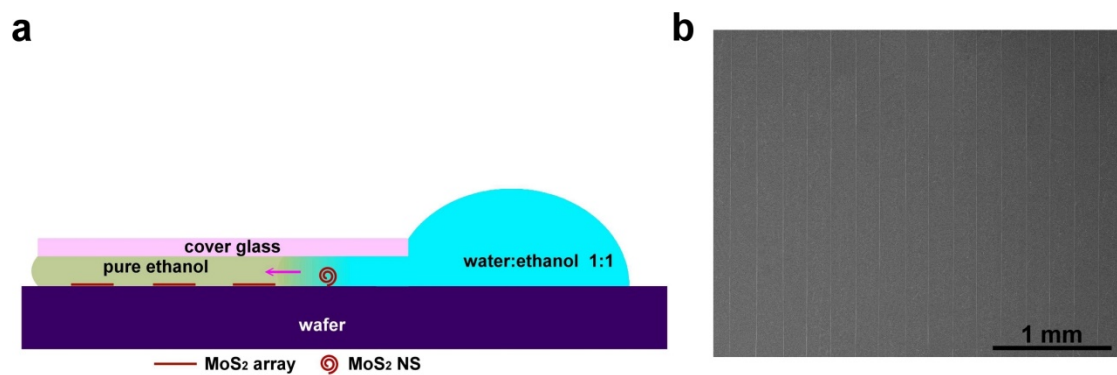
Supplementary Figure 5. **a**, The TEM image of a typical MoS₂-NS. **b**, a schematic illustration of the MoS₂-NS in (a). **c**, Potential energy analysis of a flat MoS₂ sheet (blue line), a flat MoS₂ sheet with solvent intercalation at its interface with the substrate (red dash line), and a scrolled MoS₂ sheet (red line), plotted as the function of length l .



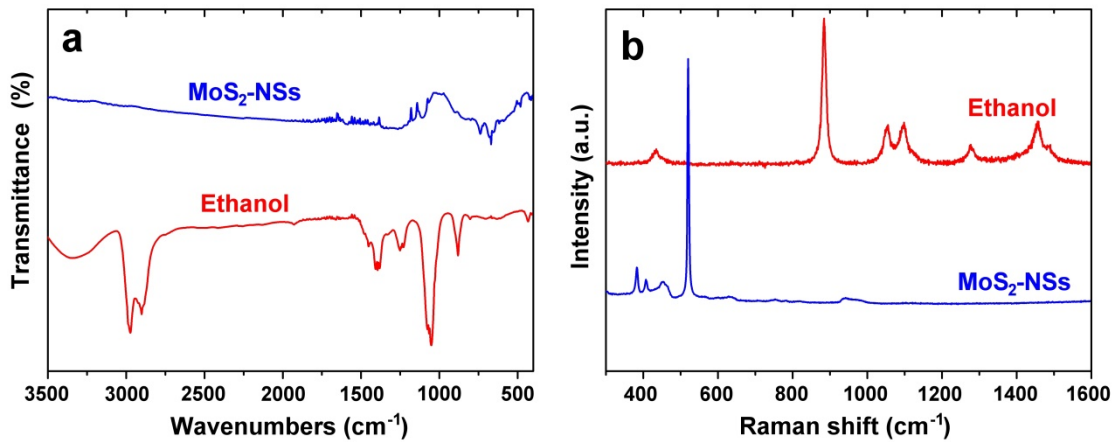
Supplementary Figure 6. SEM image of an aged MoS₂ sample on a SiO₂/Si substrate.



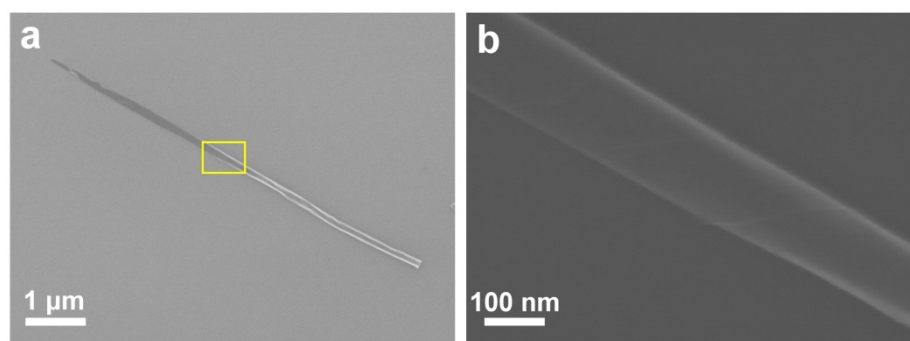
Supplementary Figure 7. Chirality of the monolayer MoS_2 single crystal scrolling.
a, SEM image of a MoS_2 -NS rolled up from a single-crystal MoS_2 monolayer. **b**, High-magnification SEM image of the rectangular area in **(a)**. **c-e**, Schematic of scrolling chirality of TMD-NSs made from single-crystal flakes. The single-crystal TMDs flakes curled along the zigzag edge. (Scale bars, 10 μm in **a** and 500 nm in **b**)



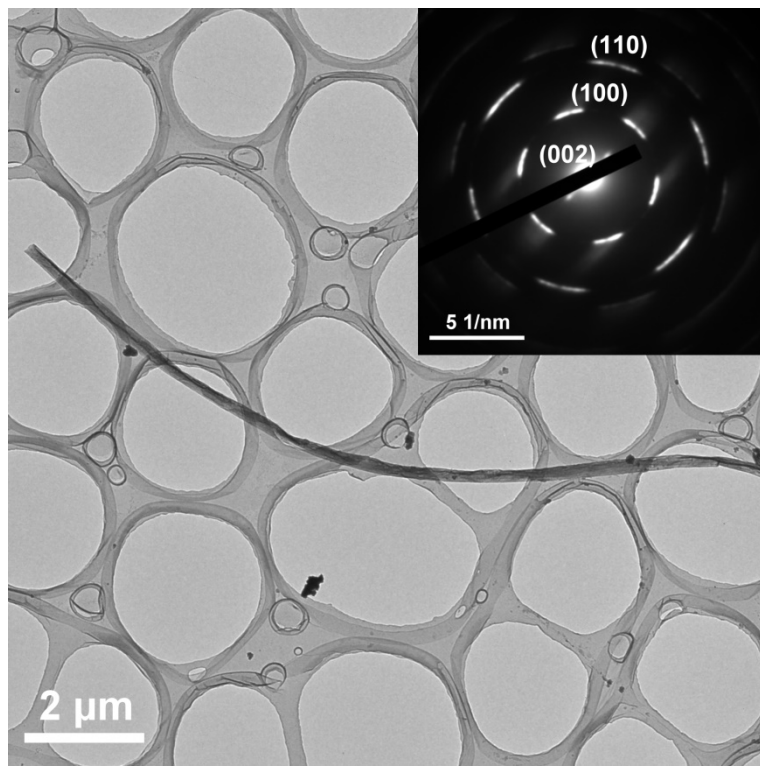
Supplementary Figure 8. **a**, Schematic of the preparation of a MoS₂-NS array. **b**, A long MoS₂-NS array with a maximum area of about 3 mm×3 mm on a SiO₂/Si substrate.



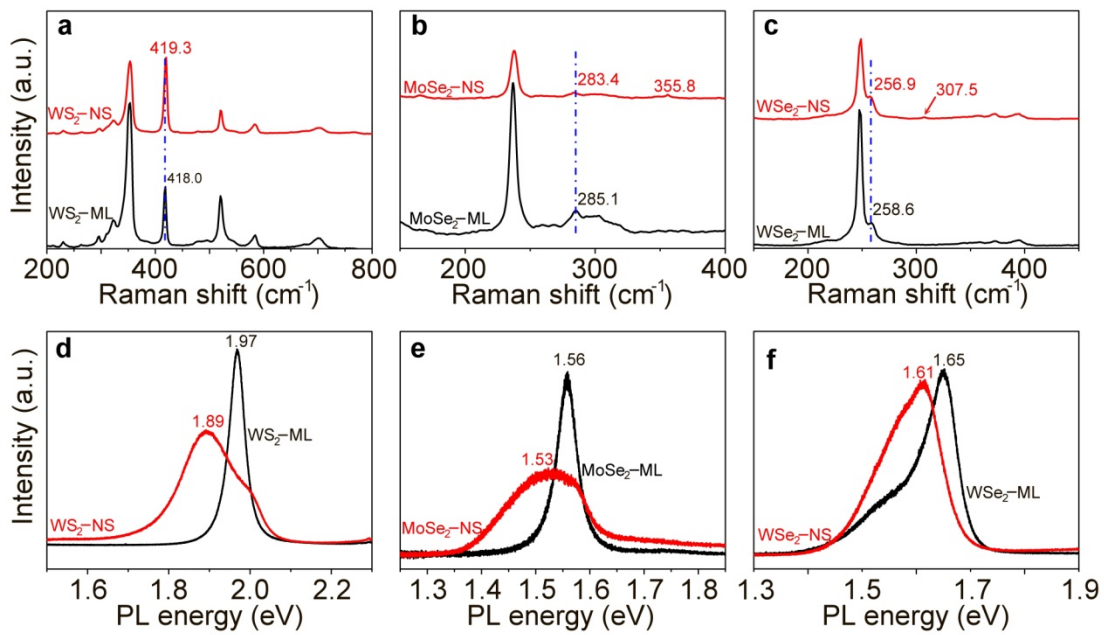
Supplementary Figure 9. Infrared (IR) and Raman analysis of MoS₂-NSs. **a**, IR spectrum of ethanol (red) and MoS₂-NSs (blue). **b**, Raman spectra of ethanol (red) and MoS₂-NSs (blue). A weak IR band at 481 cm^{-1} was assigned to Mo-S vibration. In the Raman spectra, vibration modes (at 382.9 cm^{-1} , 407.3 cm^{-1}) were clearly observed for MoS₂-NSs, without modes for ethanol in the NS. IR and Raman spectra both showed there was no residual ethanol in the nanoscrolls. The IR analysis was carried out under ambient conditions on a microscope setup (Nicolet iN10-iZ10). Raman characterization was performed with a 785 nm laser (inVia-Reflex).



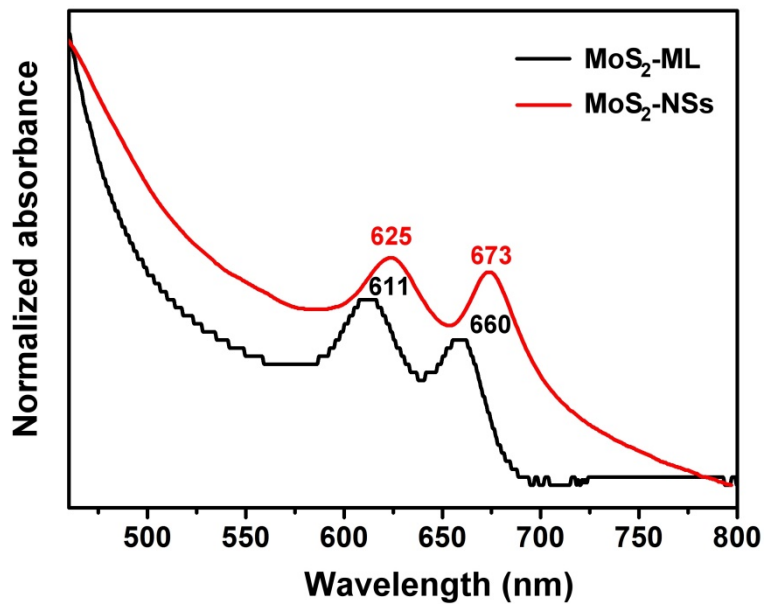
Supplementary Figure 10. **a**, SEM image of a MoS₂-NS. **b**, An enlarged image of the marked area in (a).



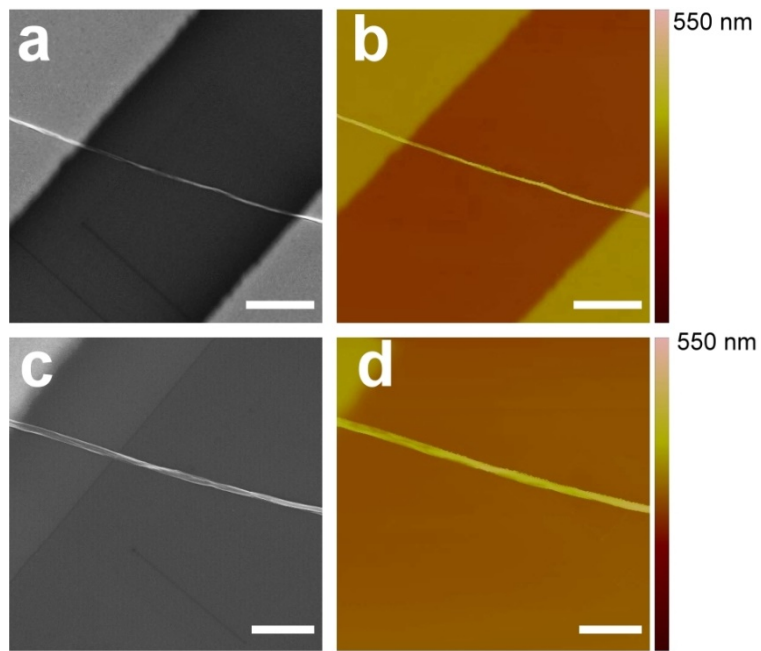
Supplementary Figure 11. TEM image and the selected-area diffraction (SAED) pattern (inset) of an individual MoS₂-NS. Two sharp diffraction spots, indexed to (002) plane, indicated the uniformity of the interlayer spacing in the NS. According to Bragg's diffraction equation, the interlayer spacing of the NS was about 6.18 Å, in good agreement with the HR-TEM observation.



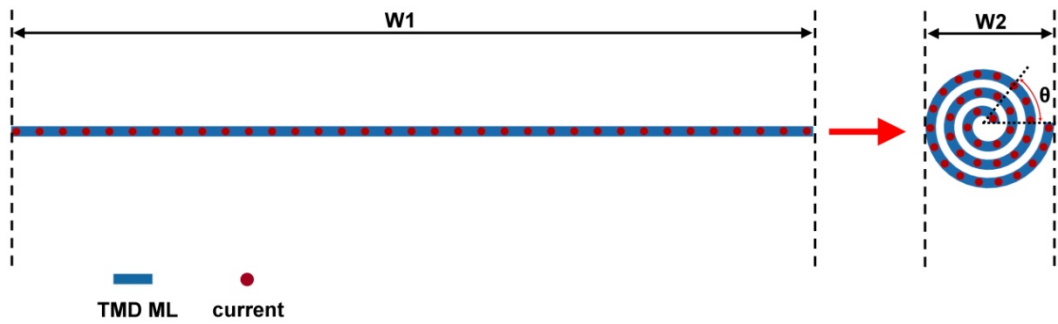
Supplementary Figure 12. Optical characterization of WS_2 -, MoSe_2 -, and WSe_2 -NSs. **a-c,** Raman spectra of CVD-grown WS_2 , MoSe_2 , and WSe_2 monolayers (ML, black) and NSs (red), respectively. **d-f,** PL spectra of CVD-grown WS_2 , MoSe_2 , and WSe_2 monolayers (black) and NSs (red) (532 nm excitation).



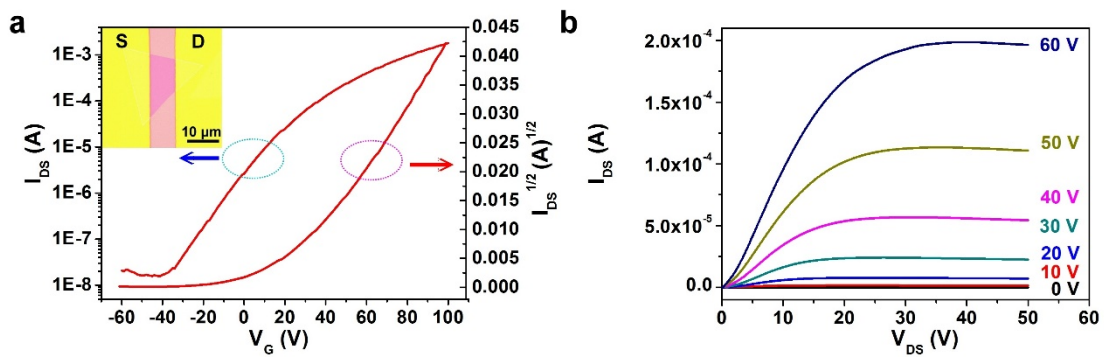
Supplementary Figure 13. Optical absorption characterization of MoS₂ monolayers (MoS₂-ML) and MoS₂-NSs. Monolayer MoS₂ and the thin film of NSs were both measured on a fused quartz substrate in an integrating sphere set-up (UV-2600). The NS film was prepared by the accumulation of the multiple transferred nanoscrolls from SiO₂/Si substrate and the spectra were normalized for better comparison. Obvious red shift in absorption resonances was observed after scrolling, corresponding to the red shift of exciton transitions in the PL spectra.



Supplementary Figure 14. High-resolution scanning electron microscope (HR-SEM) and atomic force microscope (AFM) characterization of MoS₂-NS FET in Figure 4b. **a**, HR-SEM image of the MoS₂-NS FET. **b**, AFM image of the MoS₂-NS FET showed in (a). **c**, HR-SEM image of part of the MoS₂-NS FET in (a). **d**, AFM image of the MoS₂-NS FET showed in (c). (Scale bars, 5 μ m in **a,b** and 2 μ m in **c,d**)

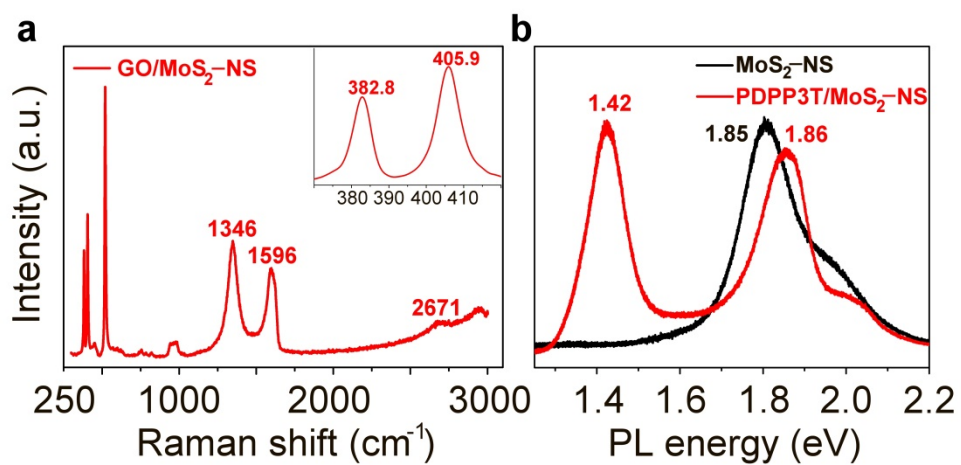


Supplementary Figure 15. The schematic of a monolayer TMD flake rolled into a NS along the conduction channel width direction. W_1 , W_2 represent the conduction channel widths of TMD flake and the NS respectively. θ is the torsion angle expressed in polar coordinates.

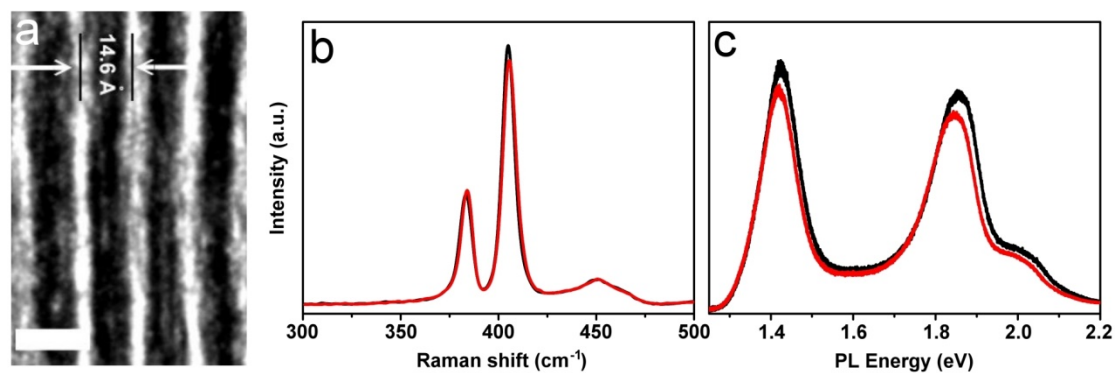


Supplementary Figure 16. Electrical characterizations of monolayer MoS₂ FETs.

a, Transfer curve of a back-gated monolayer MoS₂ FET measured in N₂ at room temperature. The source-drain bias was fixed at 60 V. Inset: Photograph of the FET device made from a monolayer MoS₂ flake grown on a SiO₂/Si substrate by CVD. The monolayer MoS₂ flake has similar dimensions as the flake that rolled into the NS in Figure 4b. **b**, Output curve of the monolayer MoS₂ FET. Experimented results show that the flake FET has a similar saturated current to that of the NS FET under the same bias. There is no significant decline in saturated current for the flakes upon scrolling process.



Supplementary Figure 17. Optical characterization of hybrid MoS₂-NSs. **a**, Raman spectrum of GO/MoS₂-NSs. The inset is a magnified view of the range of 370-420 cm⁻¹. **b**, PL spectra of MoS₂-NSs (black) and PDPP3T/MoS₂-NSs (red) (532 nm excitation).



Supplementary Figure 18. **a**, HR-TEM images of PDPP3T/MoS₂-NSs one month after the first intercalation. **b**, Raman spectra of PDPP3T/MoS₂-NSs placed in ambient condition for 0 day (black line) and one month (red line). **c**, PL spectra of PDPP3T/MoS₂-NSs placed in ambient condition for 0 day (black line) and one month (red line). (532 nm excitation)

Supplementary Notes

Supplementary Note 1. The role of immersing solution in CVD-based TMD flake scrolling

To clarify the role of the immersing solution in TMD flake scrolling, an analog experiment was carried out. CVD-grown MoS₂ flakes were transferred from growth substrate to another bare SiO₂/Si substrate with a polymer-based method. In this process, the built-in tension in the flakes can be released because of the elastic polymer support [1]. Then the transferred sample was immersed into the ethanol solution for 30 minutes. Almost no scrolls were observed in the transferred sample after the procedures above, as shown in Supplementary Fig. 1a and b. The result indicated that the tension to scroll the flake was not induced by the immersing solution. It was observed that the immersing solution here was to intercalate into the flake and the substrate, thereby weakening the adhesion between them. This was crucial for built-in tension to initiate the flake scrolling, as analyzed in theory section (Supplementary Note 2). The existence of water was found to be indispensable to the intercalation. A strong interaction of hydrogen bond can be formed between water and the growth substrate (SiO₂/Si, Si₃N₄ or sapphire), which is stronger than the Van der Waals' force between TMD flakes (hydrophobic) and the substrate. Thus after being dropped on the sample, the water tends to substitute the flakes to contact with the substrate, leading to the intercalation between flakes and the substrate. Instantaneous intercalation happened to the samples when only water used. But the sharp intercalation often caused large pieces of TMD film peeled off together from the

substrate and floated in the water, giving rise to loosely curled, disordered nanoscrolls with large film unscrolled (Supplementary Fig. 1c). A moderate intercalation speed is required for the formation of high-quality nanoscrolls. Under a low intercalation speed, the substrate can act as a template to enable the flake to scroll straightly and tightly. Mixing water with water-soluble organic solvents, such as ethanol, methanol and dimethylformamide, was observed to slow down the intercalation. When only pure organic solvent was used, the intercalation proceeded quite slowly, and even cannot be observed. Optimizing the ratio of water and organic solvents in solution, high-quality scrolling of TMD flakes can be achieved. With the same concentration of aqueous solution, the scrolling speed slightly increased with the polarity of the organic solvent. High-quality scrolling can also be obtained with different solutions at the optimized ratio, as shown in Supplementary Fig. 2.

Supplementary Note 2. Energy analysis of the formation process of a MoS₂-NS

To understand the formation mechanism of a MoS₂-NS as a result of the release of elastic energy upon solvent intercalation, we present a comparative energy analysis of flat and scrolled MoS₂ sheets on a SiO₂/Si substrate.

For a stress-free MoS₂ sheet with length of l and width w adhered on a SiO₂/Si substrate, the potential energy composes of the interfacial adhesion energy $U_A = -\gamma_1 A$, where γ_1 is the areal adhesion energy density and $A = wl$ is the contact area between MoS₂ sheet and substrate, as well as the in-plane tensile energy of the MoS₂ sheet resulted from the mismatch in thermal strain as the MoS₂/substrate system is cooled from 720-825 °C to the room temperature, which is $U_I = E_{2D}[(\alpha_1 - \alpha_2)\Delta T]^2 wl/2$. Here E_{2D} is the in-plane tensile stiffness of monolayer MoS₂ sheet, α_1 and α_2 are the thermal expansion coefficients of MoS₂ and substrate, respectively, and ΔT is the change of temperature. The total potential energy (U_f) of the hybrid with a flat MoS₂ sheet on SiO₂/Si substrate is then

$$U_f = E_{2D}[(\alpha_1 - \alpha_2)\Delta T]^2 wl/2 - \gamma_1 wl \quad (1)$$

For a scrolled MoS₂ sheet on the SiO₂/Si substrate, the total energy (U) includes the self-adhesion energy of the MoS₂ sheet $U_S = -\gamma_2(l - l_s)$, and the out-of-plane bending energy (U_B) of MoS₂,

$$U_B = \frac{\pi D}{h} \ln \left(\frac{\sqrt{lh/\pi + r_0^2}}{r_0} \right),$$

where γ_2 is interlayer adhesion energy density between MoS₂ sheet itself, $l_s = 2\pi r_0$ is the critical length of cylindrical nucleus of the scroll, h is the interlayer spacing of MoS₂-NSs, and r_0 is the radius of the cylindrical nucleus, as shown in Supplementary

Fig. 5a, b. The total potential energy of the hybrid with MoS₂-NS on SiO₂/Si substrate is then

$$U = \begin{cases} \frac{\pi D w}{h} \ln \left(\frac{\sqrt{lh / \pi + r_0^2}}{r_0} \right) & (l < 2\pi r_0) \\ \frac{\pi D w}{h} \ln \left(\frac{\sqrt{lh / \pi + r_0^2}}{r_0} \right) - \gamma_2 w(l - 2\pi r_0) & (l \geq 2\pi r_0) \end{cases} \quad (2)$$

Using the typical measured values of parameters in our previous analysis, that are ΔT about 750 K, r_0 about 10 nm (from our experimental setup), $h = 0.621$ nm, $\gamma_1 = 0.170$ J m⁻² [2], $\gamma_2 = 0.140$ J m⁻² [3], $E_{2D} = 122.30$ N m⁻¹ [4], $D = 6.29$ eV [4], $\alpha_1 = 7 \times 10^{-6}$ K⁻¹ [5] and $\alpha_2 = 2.6 \times 10^{-6}$ K⁻¹ [6]. For a flat sheet to bend into a scroll, a cylindrical nucleus has to be formed with a critical length of nucleation $l_s = 2\pi r_0$ (around 62.8 nm) as observed in our experiments, and an energy barrier $E_b = 1.9$ eV nm⁻¹, as calculated from supplementary equation 2.

As the solvent intercalation proceeds, the interlayer spacing between MoS₂ and substrate is increases and the adhesion energy γ_1 will decrease abruptly and we assume that γ_1 become zero (about 0 J m⁻²) after the delamination.

We plot the total potential energy per width for a flat MoS₂ flake (blue line), a flat MoS₂ flake with intercalated solvent (red dash line), and a scrolled MoS₂ (red line), as a function of the contour length of sheets l (Supplementary Fig. 5c). Our energy analysis shows that there is a relatively low energy barrier of 0.3 nJ m⁻¹ or 1.9 eV nm⁻¹ for the scroll to nucleate below the critical length for scroll nucleation l_s , compared with the flat MoS₂ with intercalated solvent. As shown in the inset of Supplementary Fig. 5c, as the contour length of MoS₂ sheets exceeds 0.45 μm, the potential energy of

a flat MoS₂ with solvent intercalation (red dash line) is higher than the energy barrier to form scrolled MoS₂. This result indicates that the strain energy induced from the thermal mismatch of a flat MoS₂ is high enough to activate the formation of scrolls after solvent intercalation and decreasing the adhesion energy with substrate (Supplementary Fig. 5c). It should be remarked here that the conclusion holds on the condition that γ_1 becomes lower than γ_2 after solvent intercalation.

Supplementary Note 3. Analysis of the effect of compact scroll on FET mobility

We model the cross-section of a TMD-NS as an Archimedean spiral [7], as shown in Supplementary Fig. 15. The change of the scroll radius r along the length depends on the torsion angle θ expressed in polar coordinates:

$$r = a\theta + b \quad (1)$$

where $a=t/2\pi$ is the spiral constant; t is the radius change per one full turn, approximately equal to the interlayer distance in the NS; b is the scroll radius at $\theta=0$, i.e., the inner radius of the NS. As determined from TEM images, the t is approximately 0.6 nm and b is in the range of 5-20 nm for TMDs-NSs.

The arc length s of the Archimedean spiral is an integral by θ .

$$s = \int_0^s ds = \int_0^\theta \sqrt{(dr)^2 + (r d\theta)^2} \quad (2)$$

Substitution of supplementary equation (1) into supplementary equation (2) yields

$$s = \int_0^\theta \sqrt{a^2 + (a\theta + b)^2} d\theta \quad (3)$$

Based on the integral formula, the supplementary equation (3) can be computed as

$$\begin{aligned} s = & \frac{a\theta + b}{2a} \sqrt{a^2 + (a\theta + b)^2} + \frac{a}{2} \ln \left[b + a\theta + \sqrt{a^2 + (a\theta + b)^2} \right] - \frac{b}{2a} \sqrt{a^2 + b^2} \\ & - \frac{a}{2} \ln \left(b + \sqrt{a^2 + b^2} \right) \end{aligned} \quad (4)$$

As shown in Supplementary Fig. 15, a TMD flake scrolled into a NS along one edge.

The conduction channel width $W1$ for the TMD flake is just the arc length s of the NS spiral, while the conduction channel width $W2$ for the NS is equal to its diameter $2r$.

Thus, the ratio of the conduction channel widths before and after scrolling can be described as

$$\frac{W1}{W2} = \frac{s}{2r} \quad (5)$$

Substitution of supplementary equations (1) and (4) into supplementary equation (2)

yields

$$\begin{aligned} \frac{W1}{W2} &= \frac{1}{4a} \sqrt{a^2 + (a\theta + b)^2} + \frac{a}{4(a\theta + b)} \ln \left[b + a\theta + \sqrt{a^2 + (a\theta + b)^2} \right] \\ &\quad - \frac{b}{4a(a\theta + b)} \sqrt{a^2 + b^2} - \frac{a}{4(a\theta + b)} \ln \left(b + \sqrt{a^2 + b^2} \right) \end{aligned} \quad (6)$$

Given that a is relatively small value of ~ 0.095 , the supplementary equation (6) is simplified to

$$\frac{W1}{W2} = \frac{\theta}{4} - \frac{b^2}{4a(a\theta + b)} + \frac{b}{4a} \quad (7)$$

Assuming that the flake rolled by full turns with $\theta=2n\pi$ (n , the scroll turns, i.e., layer number in the NS), the dependence of the ratio of the conduction channel widths on the scroll turns can be expressed as follows:

$$\frac{W1}{W2} = \frac{n\pi}{2} - \frac{b^2}{4a(2an\pi + b)} + \frac{b}{4a} \quad (8)$$

Supplementary References

1. Amani, M. et al. High luminescence efficiency in MoS₂ grown by chemical vapor deposition. *ACS Nano* **10**, 6535–6541 (2016).
2. Deng, S. et al. Adhesion energy of MoS₂ thin films on silicon-based substrates determined via the attributes of a single MoS₂ wrinkle. *ACS Appl. Mater. Interfaces* **9**, 7812–7818 (2017).
3. Li, H., Wang, J., Gao, S. et al. Superlubricity between MoS₂ monolayers. *Adv. Mater.* **29**, 1701474 (2017).
4. Gao, E., Xu, Z. Thin-shell thickness of two-dimensional materials. *J. Appl. Mech.* **82**, 121012 (2015).
5. Sevik, C. Assessment on lattice thermal properties of two-dimensional honeycomb structures: Graphene, *h*-BN, *h*-MoS₂, and *h*-MoSe₂. *Phys. Rev. B* **89**, 035422 (2014).
6. Calizo, I., Balandin, A. A., Bao, W., Miao, F., Lau, C. N. Temperature dependence of the Raman spectra of graphene and graphene multilayers. *Nano Lett.* **7**, 2645–2649 (2007)
7. Krasilin, A. A. & Gusarov, V. V. Energy of formation of chrysotile nanotubes. *Russ. J. Gen. Chem.* **84**, 2359–2363 (2014).